Intermetallics 91 (2017) 95–99

Contents lists available at ScienceDirect

Intermetallics

journal homepage: www.elsevier.com/locate/intermet

Electric field gradient analysis of RIn_3 and RSn_3 compounds (R = La, Ce, Pr and Nd)

M. Shafiq[a,b,*], M. Yazdani-Kachoei[c], S. Jalali-Asadabadi[c], Iftikhar Ahmad[a,b]

[a] Department of Physics, Abbottabad University of Science and Technology, Havelian, Abbottabad, Pakistan
[b] Center for Computational Materials Science, University of Malakand, Pakistan
[c] Department of Physics, Faculty of Sciences, University of Isfahan, HezarGerib Avenue, Isfahan 81744-73441, Iran

ARTICLE INFO

Keywords:
Electric field gradient
Rare-earth intermetallics
Strongly correlated
Spin-orbit coupling

ABSTRACT

In this paper we explore the electronic charge distribution at different atomic sites in the rare-earth intermetallics RIn_3 and RSn_3 (R = La, Ce, Pr and Nd) using the analysis of the electric field gradients (EFGs) calculated by the FP-LAPW + lo method. The *f*-state in these compounds makes them strongly correlated systems, therefore the exchange and correlations are treated with GGA + U along with the GGA whereas GGA + SOC is also used to treat the relativistic effects. The calculated EFG values are consistent with the experimental results of the Mössbauer spectroscopy for $LaSn_3$, $CeSn_3$, $CeIn_3$, $PrSn_3$ and $NdSn_3$ and therefore we expect that our calculated values for the remaining compounds will be also consistent with the experimental results. The anisotropy of the charge distribution in the vicinity of a nucleus causes EFG and therefore the orbitals contribution of EFG i.e., V_{zz}^{p-p}, V_{zz}^{s-d}, V_{zz}^{d-d}, V_{zz}^{p-f} and V_{zz}^{f-f} are evaluated for nonmagnetic and AMF phases using GGA, GGA + U and GGA + SOC.

1. Introduction

The analyses of the nucleus-electron interactions beyond the nuclear point charge approximation provides useful information in condensed matter physics. Electric field gradient (EFG) is one of those physical quantities, which is obtained from this analysis. The EFG serves as a powerful tool to measure the interaction between atomic nucleus and electronic charge density around the nucleus [1]. The EFG takes place due to the rate of Coulomb potential change at the nucleus and the nature of EFG is very sensitive to a slight change in bonding, structure and dynamics of an atom [2,3]. These properties are highly dependent upon the symmetry of the electronic charge density of core electrons [4] and valence electrons [5]. EFG can be used as a measure of the degree of electron's localization in the solids [6]. Experimentally EFG cannot be measured directly, but it can be obtained by different techniques such as Mössbauer spectroscopy (MS), perturbed angular correlation (PAC) spectroscopy, nuclear magnetic resonance (NMR), and nuclear quadrupole resonance (NQR) [7]. However, theoretically EFG can be accurately predicted by ab-initio method using density functional theory (DFT) [8]. Various theoretical studies are reported in the literature on the EFG in a variety of materials, for example, intermetallics [9], metal complexes [10], magnetic [11] or multiferroic compounds [12].

Rare-earth (RE) intermetallic compounds RIn_3 and RSn_3 (R = La, Ce, Pr and Nd) have cubic $AuCu_3$-type structure. The corner site is occupied by R atom having cubic symmetry m-3m and the face centered sites are occupied by X atoms having tetragonal symmetry 4/mmm [6].

The strongly correlated rare-earth (RE) intermetallic compounds RX_3 (R = rare-earth and X = In, Sn) have attracted special attention because of their interesting physical, electronic, and mechanical properties, which make them significant materials for technological and industrial applications [13–15]. Some of the attractive features of these compounds are their low superconducting transition temperature, magnetic susceptibility and thermoelectric power as a function of their electron concentration [16,17]. The RX_3 compounds are also significant due to their simple crystal structure, stability in the cubic structure over a wide range of pressures [18] and more favorable structure for superconductivity than lower symmetry [19].

The rare-earth elements have different occupation numbers for the shallow inner 4*f* shell, ranging from 0 to 14 through the series. This changing of 4*f* occupation determines a wide range of different physical properties of rare-earth elements and compounds. Due to the unfilled 4*f* shells of rare-earth atoms, it is a challenging problem to obtain an accurate theoretical description of the lanthanide based compounds [15,20]. The rare earth intermetallic compounds RX_3 show certain trends in the lattice constant value across the lanthanide series and

* Corresponding author. Department of Physics, Abbottabad University of Science and Technology, Havelian, Abbottabad, Pakistan.
E-mail address: shafiqdurraniuom@gmail.com (M. Shafiq).

http://dx.doi.org/10.1016/j.intermet.2017.08.014
Received 23 May 2017; Received in revised form 16 August 2017; Accepted 21 August 2017
0966-9795/ © 2017 Elsevier Ltd. All rights reserved.

exhibit the characteristic lanthanide contraction. In RX_3 compounds from La to Lu, the rare-earth element form trivalent ions except Eu and Yb, which form divalent oxidation. The lattice constant of divalent ion (Eu andYb) is larger than trivalent ion by almost 10% [19,21]. The structural and magnetic properties of RIn_3 (R = Ce, Pr, Nd, Gd, Tb, Dy, Ho, Er, and Tm) compounds have been reported by Buschow et al. [22] and the magnetic behavior of RSn_3 (R = Ce, Pr, Nd, Sm, and Gd) have been investigated by Tsuchida and Wallace [23]. From the magnetic measurement it was observed that most of RIn_3 and RSn_3 compounds have antiferromagnetic (AFM) ordering with the exceptional Pauli paramagneticmaterial $LaIn_3$, and paramagnetic materiales $LaSn_3$, $CeSn_3$ and $PrIn_3$ [24–26]. The structural, electronic and magnetic properties of RSn_3 compounds (R = La, Ce, Pr, Nd, Sm, Eu, Gd, Yb) have been investigated using the 23.8 keV Mössbauer resonance of ^{119}Sn [27]. The Fermi surface properties and the de Haas–van Alphen (dHvA) effect in RX_3 compounds were reported by Ōnuki and Settai [26].

In this paper we explore the electric field gradients of RX_3 series (X = In and Sn, X = La, Ce, Pr and Nd) using ab-initio density functional theory calculations to better understand the physics and chemistry of these compounds due to the distribution of the electronic charge around the nucleus and nuclei-electrons interaction. The calculations are carried out with the all electron full potential linearized augmented plane waves plus local orbital (FP-LAPW + lo) method within the framework of the density functional theory (DFT), where the correlation affects are treated with the Hubbard potential and the relativistic effects are considered by the spin-orbit coupling.

2. Method of calculations

In the present work, the calculations have been performed by using the density functional theory (DFT) as implemented in the WIEN2k code [28] employing the full potential linearized augmented plane waves plus local orbitals (FP-LAPW + lo) method [29]. The exchange correlation effects are treated by the generalized gradient approximation (GGA) [30] with and without including spin effects.

The most popular approximations for the treatment of exchange correlation functional are LDA and the GGA. However, in most cases the results of these schemes are not consistence with the experimental values. As lanthanides are strongly correlated systems with localized 4*f* electrons [11,31], to obtain the exact electronic nature of the compounds under consideration, we used GGA + U methods [32]. The DFT + U method is based on the Hubbard model, which treats the strongly correlated electron systems with an orbital dependent potential of Coulomb and exchange interactions [41]. The optimized values of the U parameter are obtained by varying U, step by step.

Fig. 1 shows the effect of U on the EFG value of $CeIn_3$. It is clear from the figure that the value of EFG decreases with increase in U, consequently the difference of the calculated value decreases from the experimental results. The value of EFG at 6.5 eV is closer than the other values of U, beyond 6.5 eV the value of EFG again increases. Therefore, we select U = 6.5 eV for our calculation. Furthermore, spin-orbit coupling (SOC) is included to treat the relativistic effects. The SOC are included by a second variational method [33]. The second variational method, which makes use of the scalar-relativistic basis, based on the reduction of the original basis. In the first step of this approach, the scalar-relativistic part of the Hamiltonian is diagonalized in the scalar-relativistic basis. In the second step the full Hamiltonian matrix including SOC is constructed using the eigen functions of the first step Hamiltonian. Once the effects of spin-orbit coupling included, the full Hamiltonian can be written as:

$$H\tilde{\psi} = \varepsilon\tilde{\psi} + H_{so}\tilde{\psi} \tag{1}$$

where H_{so} is spin-orbit Hamiltonian and given by Ref. [34]:

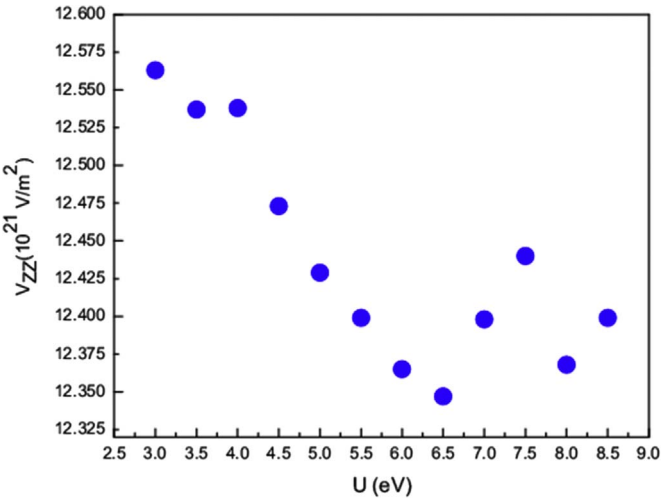

Fig. 1. The Electric field gradient of $CeIn_3$ using different Hubbard parameters GGA + U.

$$H_{so} = \frac{\hbar}{2Mc^2}\frac{1}{r}\frac{dV}{dr}\begin{pmatrix}\vec{\sigma}\vec{l} & 0\\ 0 & 0\end{pmatrix} \tag{2}$$

with $\vec{\sigma}$ is Pauli spin matrices.

The radii of the muffin-tin spheres have been chosen as 2.50 a.u for the rare-earth elements as well as for Sn and In. To achieve convergence, the basis set is expanded in terms of plane waves up to $R_{MT}K_{max} = 7$. For the valence wave function inside muffin-tin spheres, the maximum value of the angular momentum is considered as $l_{max} = 10$. In the interstitial region, the charge density is Fourier expanded up to $G_{max} = 12$. The convergence of the total energy is tested and hence the total energy is converged for 6000 k-points with a dense k mesh of 165 k-points in the irreducible wedge of the Brillouin zone with a grid size of 18 × 18 × 18.

3. Results and discussion

A nucleus with the nuclear spin quantum number $I \geq 1$ possesses nuclear quadrupole moment Q, which can interact with the electric field gradient (EFG). The EFG is a traceless symmetric tensor of rank 2 with five independent components and originates due to the deviation of the electron charge distribution from the spherical distribution in the vicinity of the nucleus (≤0.2 Å) [6]. In particular, EFG is defined as the second derivative of a classical electrostatic potential with respect to Cartesian coordinates $V_{ij} = \partial^2 V/(\partial x_i \partial x_j)$ at nuclear position. The two main independent components are principle component V_{zz} and asymmetry parameter $\eta = (V_{xx} - V_{yy})/V_{zz}$, where the standard convention $|V_{zz}| \geq |V_{yy}| \geq |V_{xx}|$ is chosen for principle axes. This also guarantees that η varies between 0 (axially symmetric) and 1 ($V_{xx} = 0$) [1,35]. These two components are used in the analysis of the EFG measurements. In the principle axes system where EFG tensor is diagonal, the main component V_{zz} of EFG has been obtained by using the following relation [36]:

$$V_{ZZ} = \lim_{r\to 0}\sqrt{\frac{5}{4\pi}}\frac{V_{20}}{r^2} \tag{3}$$

where V_{20} is the radial potential and is given by Ref. [36]:

$$V_{20}(r=0) = \frac{4\pi}{5}\int_0^{R_{MT}}\frac{\rho_{20}}{r}dr - \frac{4\pi}{5}\int_0^{R_{MT}}\frac{\rho_{20}}{r^3}\left(\frac{r}{R_{MT}}\right)^5 r^2 dr + 4\pi\sum_K V(\hat{K})J_2(KR_{MT})Y_{20}(\hat{K}) \tag{4}$$

where J_2 is the spherical Bessel function, Y_{20} is the spherical harmonic for $l = 2$, $m = 0$ and ρ_{20} is the component of charge density, ρ_{LM} for L = 2, M = 0 when it is expressed by lattice harmonics, i.e., LM form.

Table 1
Calculated main component of the EFG (V_{zz}^{tot}), valence part (V_{zz}^{val}) and lattice part (V_{zz}^{latt}) (in 10^{21} V/m^2), at In and Sn sites for nonmagnetic phase compared with the available experimental and theoretical EFG values.

Comp.	site		GGA	GGA + SOC	Other	Exp.
$LaIn_3$	In	V_{zz}^{tot}	11.914	11.833	13.5[b]	
	In	V_{zz}^{val}	11.945	12.084		
	In	V_{zz}^{latt}	−0.031	−0.251		
$PrIn_3$	In	V_{zz}^{tot}	12.832	12.115		
	In	V_{zz}^{val}	12.853	13.096		
	In	V_{zz}^{latt}	−0.021	−0.981		
$LaSn_3$	Sn	V_{zz}^{tot}	16.719	16.945		16.89[a]
	Sn	V_{zz}^{val}	16.761	17.247		
	Sn	V_{zz}^{latt}	−0.042	−0.302		
$CeSn_3$	Sn	V_{zz}^{tot}	18.487	18.546		17.97[a]
	Sn	V_{zz}^{val}	18.518	18.863		
	Sn	V_{zz}^{latt}	−0.031	−0.317		

[a] Ref [27].
[b] Ref. [40].

The first term in Eq. (2) is known as valence contribution of EFG (V_{zz}^{Val}). V_{zz}^{Val} comes from the non-spherical electron density of the valence and semicore electrons in Muffin-tin spheres. The sum of the second and third terms represents the lattice contribution of EFG and V_{zz}^{latt} arises from the outside of the Muffin-tin spheres and interstitial region.

The calculated values of the largest component of the EFGs (V_{zz}^{tot}) and their valence (V_{zz}^{val}) and lattice (V_{zz}^{latt}) contributions for $LaIn_3$, $PrIn_3$, $LaSn_3$ and $CeSn_3$ compounds using GGA and GGA + SOC are presented in Table 1. The calculated values of EFG's are also compared with the experimental values obtained from Mössbauer spectroscopy [27]. As $LaIn_3$, $PrIn_3$, $LaSn_3$ and $CeSn_3$ compounds exist in paramagnetic phase [24–26], therefore as a first approximation the calculations for these compounds are performed in nonmagnetic phase. It is clear from Table 1 that in nonmagnaetic phase, the GGA functional provides good results, consistent with the experimental values for these compounds. In these compounds only the In and Sn with nuclei of non-cubic symmetry, exhibit the electric quadrupole interaction, and have nonzero EFG. At rare-earth elements La, Ce and Pr sites (Table 1) the EFGs are zero due to the cubic symmetry for all the nonmagnetic phase with and without SOC effects. The results show that, the magnitude of the EFGs for $LaIn_3$ and $PrIn_3$ are closer to each other, hence the electron density distributions near the In nuclei are similar. The same also holds for Sn nuclei in $LaSn_3$ and $CeSn_3$. The total EFG (V_{zz}^{tot}) of In and Sn sites in $LaIn_3$, $PrIn_3$, $LaSn_3$ and $CeSn_3$ is positive which predict the prolate distribution of electrons.

Table 2 represents the calculated values of the EFG's (V_{zz}^{tot}) and their related valence (V_{zz}^{val}) and lattice (V_{zz}^{latt}) contributions for $CeIn_3$, $NdIn_3$, $PrSn_3$ and $NdSn_3$ compounds. RIn_3 and RSn_3 compounds with R = Ce, Pr and Nd, exist in AFM phase [37–39]. The calculations for these compounds are performed in the magnetically split AFM phase by using GGA, GGA + U and GGA + SOC. The results listed in Table 2 are compared with the available experimental results. It is evident from Table 2 that our calculated results by GGA and GGA + SOC approaches overestimate the EFG values with respect to the experimental results. Our theoretical calculations for EFG values performed with GGA + U agree well with the experimental results. As lanthanides are strongly correlated systems due to their 4*f* electrons, hence the better agreement confirms that we have properly treated correlations among the 4*f* electrons within GGA + U calculations. Table 2 also indicates nonzero EFG values at rare-earth (Ce, Pr and Nd) site. The nonzero EFG values are due to the fact that AFM ordering can cause a slight deviation from the cubic symmetry around the rare-earth atom. The total EFG (V_{zz}^{tot}) of In and Sn sites in $CeIn_3$, $NdIn_3$, $PrSn_3$ and $NdSn_3$ compounds is positive

Table 2
Calculated main component of the EFG (V_{zz}^{tot}), valence part (V_{zz}^{val}) and lattice part (V_{zz}^{latt}) (in 10^{21} V/m^2), at In and Sn sites for AFM phase compared with the available experimental and theoretical EFG values.

Comp.	Site		GGA	GGA + U	GGA + SOC	others	Exp.
$CeIn_3$	Ce	V_{zz}^{tot}	0.023	−2.739	−0.042		
	In		13.691	12.347	12.755	14.7[c]12.49[d]	11.60[b]
	Ce	V_{zz}^{val}	0.025	−2.732	0.244		
	In		13.716	12.337	13.245		
	Ce	V_{zz}^{latt}	−0.002	−0.007	−0.286		
	In		−0.025	0.010	−0.490		
$NdIn_3$	Nd	V_{zz}^{tot}	−0.134	−1.339	0.124		
	In		13.362	12.459	12.923		
	Nd	V_{zz}^{val}	−0.135	−1.435	0.777		
	In		13.386	12.784	12.982		
	Nd	V_{zz}^{latt}	0.001	−0.004	−0.653		
	In		−0.030	−0.025	−0.059		
$PrSn_3$	Pr	V_{zz}^{tot}	−0.284	−2.629	−0.248		
	Sn		17.174	16.466	17.214		15.65[a]
	Pr	V_{zz}^{val}	−0.285	−2.627	−0.162		
	Sn		17.206	16.499	17.402		
	Pr	V_{zz}^{latt}	0.001	−0.002	−0.086		
	Sn		−0.032	−0.033	−0.188		
$NdSn_3$	Nd	V_{zz}^{tot}	−0.207	−1.616	−0.316		
	Sn		17.217	16.981	17.305		16.58[a]
	Nd	V_{zz}^{val}	−0.208	−1.614	0.251		
	Sn		17.247	17.014	17.723		
	Nd	V_{zz}^{latt}	0.001	−0.002	−0.567		
	Sn		−0.030	−0.033	−0.418		

[a] Ref. [27].
[b] Ref. [41].
[c] Ref. [40].
[d] Ref. [11].

which predict the prolate distribution of electrons. The positive value of total EFG (V_{zz}^{tot}) of rare-earth element Ce in $CeIn_3$ predict the prolate shape of orbital while the negative value of V_{zz}^{tot} of rare-earth element Nd in $NdIn_3$ and $NdSn_3$, and Pr in $PrSn_3$ indicate the oblate nuclear charge distribution.

The main contribution of the EFG is due to the anisotropy of the charge distribution in the vicinity of a nucleus. In order to further analyze these contributions, we evaluate the orbital contributions V_{zz}^{p-p}, V_{zz}^{s-d}, V_{zz}^{d-d}, V_{zz}^{p-f}, V_{zz}^{f-f}. Fig. 2 shows the orbital contributions of the nonmagnetic phase and AMF phase of the compounds under consideration using GGA, GGA + U and GGA + SOC. It is clear from the figure that the *p-p* contribution is dominant at In and Sn sites in case of all approximations for both nonmagnetic and AFM phases. In RIn_3 and RSn_3 compounds, In and Sn atom which has 4*d* complete shell, the *d* orbital is spherical symmetric. The 5*p* contribution is the consequences of the non spherical distribution of charge as compared to rare-earth element. The dominant value of *p-p* contribution indicates that, the electron density of 5*p* electrons around the indium (in RIn_3) and tin (in RSn_3) atoms is identical across the series and independent of rare-earth atom. It is also seen from Fig. 2, that *s-d*, *d-d*, *p-f* and *f-f* contributions are very small as compared to the valance EFGs and are comparable in magnitude.

Fig. 3 represents the orbital contribution of Ce atom in $CeIn_3$. It is evident from the figure that at rare-earth (Ce in this case) site the *f-f* contribution dominates as compared to the *p*-states in the compounds under investigation. The valence character of *f-f* orbitals of Ce site specifies the non spherical distribution of nuclear charge. This demonstrates that at rare-earth nuclei (Ce, Pr, and Nd), the main contribution to valence EFGs are originated by 4*f* states.

4. Conclusions

In summary we have calculated the electric field gradients (EFGs) and their valence contributions at rare-earth and In/Sn sites for RIn_3 and RSn_3 (R = La, Ce, Pr and Nd) using FP-LAPW + lo method with

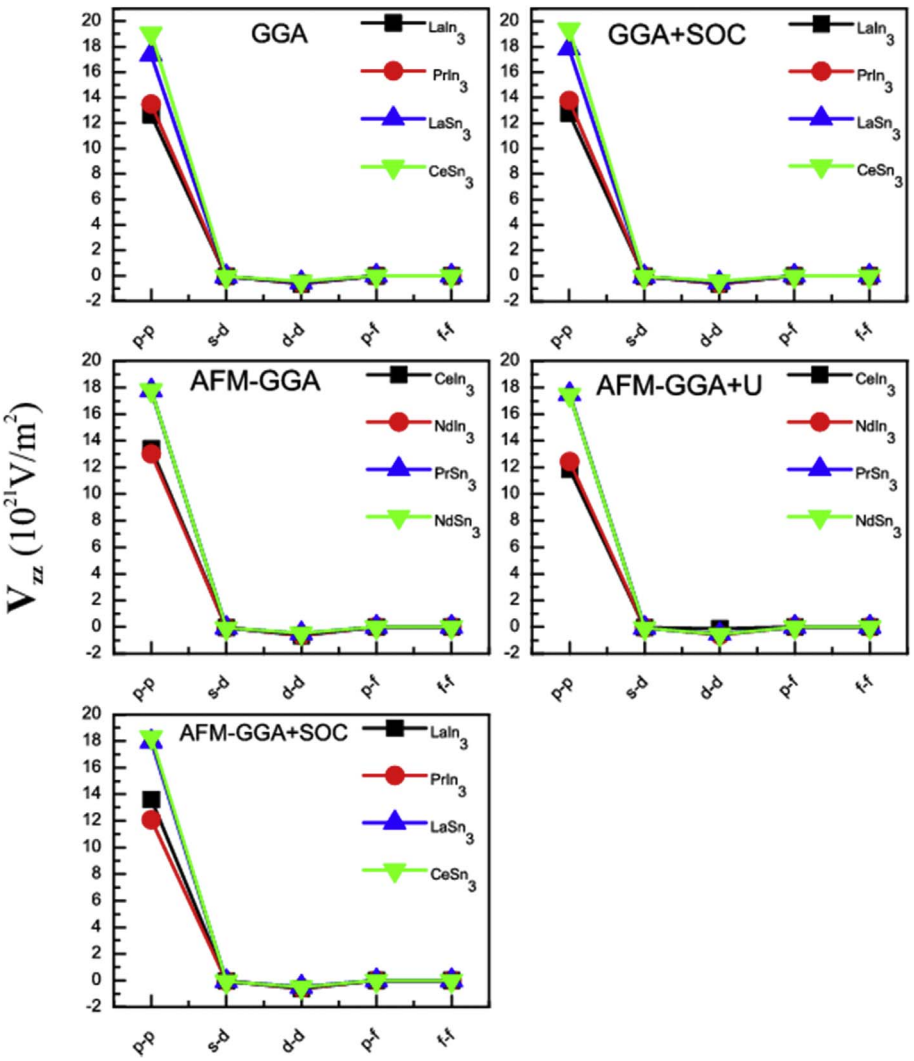

Fig. 2. Decomposition of the valence EFG into *p-p*, *s-d*, *d-d*, *p-f* and *f-f* contributions calculated for nonmagnetic and AFM phases with GGA, GGA + SOC and GGA + U.

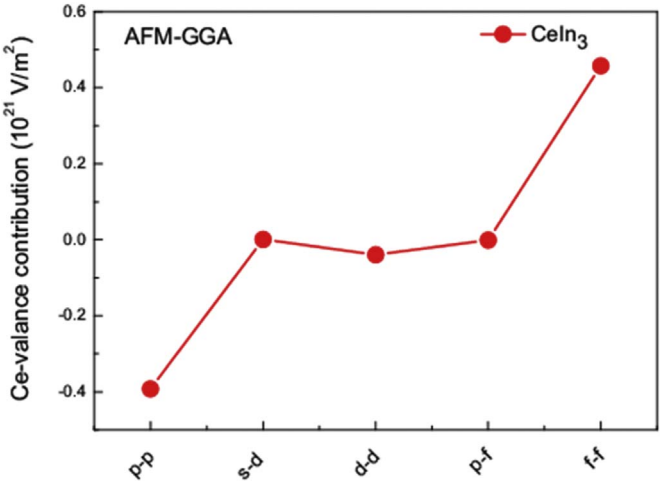

Fig. 3. Decomposition of valence EFG at Ce site for AFM phase.

various exchange-correlation functionals. Our analysis concludes that the main EFG contributions to In and Sn sites come mainly from 5*p* state. At rare-earth site the valance EFG is predominantly from 4*f* states. From the orbital contributions it is evident that that the *p-p* contribution is dominant at In and Sn sites in case of all approximations for both nonmagnetic and AFM phases. Although, EFG is a very sensitive quantity but even then our calculated EFG parameters for $LaSn_3$, $CeSn_3$, $CeIn_3$, $PrSn_3$ and $NdSn_3$ materials are consistent with the experimental results of the Mössbauer spectroscopy. This comparison concludes the effectiveness of the theoretical tools for the accurate EFG calculations. Furthermore, on the basis of this former conclusion we also conclude that the calculated values of EFGs for $LaIn_3$, $PrSn_3$ and $NdSn_3$ compounds will be also consistent with the experimental results.

References

[1] E. Ghasemikhah, S.J. Asadabadi, I. Ahmad, M. Yazdani-Kachoei, Ab initio studies of electric field gradients and magnetic properties of uranium dipnicties, RSC Adv. 5 (2015) 37592–37602.
[2] J.N. Gonçalves, A. Stroppa, J.G. Correia, T. Butz, S. Picozzi, A.S. Fenta, V.S. Amaral, Ab-initio study of the relation between electric polarization and electric field gradients in ferroelectrics, Phys. Rev. B 86 (2012) 035145.
[3] J. Autschbach, S. Zheng, R.W. Schurko, Analysis of electric field gradient tensors at quadrupolar nuclei in common structural motifs, Concepts Magn. Reson. Part A 36A (2010) 84–126.
[4] J. Yu, A.J. Freeman, R. Podloucky, P. Herzig, P. Weinberger, Origin of electric-field gradients in high-temperature superconductors: YBa_2Cu_3, Phys. Rev. B 43 (1991) 532–541.
[5] K. Schwarz, C. Ambrosch-Draxl, P. Blaha, Charge distribution and electric-field gradients in $YBa_2Cu_3O_{7-x}$, Phys. Rev. B 42 (1990) 2051–2061.
[6] S.J. Asadabadi, S. Cottenier, H. Akbarzadeh, R. Saki, M. Rots, Valency of rare earths in RIn_3 and RSn_3: *Ab initio* analysis of electric-field gradients, Phys. Rev. B 66 (2002) 195103.
[7] G. Schatz, A. Weidinger, Nuclear Condensed Matter Physics: Nuclear Methods and Applications, Wiley, New York, 1996.
[8] P. Blaha, K. Schwarz, P. Herzig, First-Principles calculation of the electric field gradient of Li_3N, Phys. Rev. Lett. 54 (1985) 1192–1195.

[9] F. Haarmann, K. Koch, P. Jeglic, H. Rosner, Y. Grin, NMR Spectroscopy of intermetallic compounds: an experimental and theoretical approach to local atomic arrangements in binary gallides, Chem. Eur. J. 17 (2011) 7560–7568.

[10] R. Bjornsson, M. Buhl, Electric field gradients of transition metal complexes from density functional theory: assessment of functionals, geometries and basis sets, Dalton Trans. 39 (2010) 5319–5324.

[11] S.J. Asadabadi, Electronic structure and electric-field gradient analysis in $CeIn_3$, Phys. Rev. B 75 (2007) 205130.

[12] A.M.L. Lopes, G.N.P. Oliveira, T.M. Mendonça, J.A. Moreira, A. Almeida, J.P. Araújo, V.S. Amaral, J.G. Correia, Local distortions in multiferroic $AgCrO_2$ triangular spin lattice, Phys. Rev. B 84 (2011) 014434.

[13] S. Lebegue, S. Svane, M. Katsnelson, I. Lichenstein, O. Eriksson, Multiplet effects in the electronic structure of light rare-earth metals, Phys. Rev. B 74 (2006) 045114.

[14] M. Shafiq, I. Ahmad, S.J. Asadabadi, Theoretical studies of strongly correlated rare-earth intermetallics RIn_3 and RSn_3 (R = Sm, Eu, and Gd), J. Appl. Phys. 116 (2014) 103905.

[15] M. Shafiq, I. Ahmad, S.J. Asadabadi, Mechanical properties and variation in SOC going from La to Nd in intermetallic RIn_3 and RSn_3 (R = La, Ce, Pr, Nd), RSC Adv. 5 (2015) 39416.

[16] S. Ram, V. Kanchana, G. Vaitheeswaran, A. Svane, S.B. Dugdale, N.E. Christensen, Electronic topological transition in $LaSn_3$ under pressure, Phys. Rev. B 85 (2012) 17453.

[17] S. Ram, V. Kanchana, A. Svane, S.B. Dugdale, N.E. Christensen, Fermi surface properties of AB_3 (A = Y, La; B = Pb, In, Tl) intermetallics compounds under pressure, J. Phys. Condens. Matter 25 (2013) 155501.

[18] N.V.C. Shekar, P.C. Sahu, Pressure induced structural behavior in f-electron based AB, AB_2 and AB_3 intermetallics, J. Mater. Sci. 41 (2006) 3207–3228.

[19] I.R. Harris, G.V. Raynor, Rare earth intermediate phases: I. Phases formed with tin and Indium, J. Less Common Met. 9 (1965) 7–19.

[20] N. Yakovkin, T. Komesu, P.A. Dowben, Band structure of strained Gd(000) films, Phys.Rev B. 66 (2002) 035406.

[21] K.A. Gschneidner Jr., Physical properties and interrelationships of metallic and semimetallic elements, Solid State Phys. 16 (1964) 275–426.

[22] K.H.J. Buschow, The magnetic properties of the compound Dy_3Al_2, Phys. Lett. A 29 (1969) 12–13.

[23] T. Tsuchida, W.E. Wallace, Magnetic characteristics of lanthanide elements combined with tin, lead, and indium, J. Chem. Phys. 43 (1965) 3811–3814.

[24] I. Umehara, N. Nagai, Y. Ōnuki, High field Magnetoresistance and de Haas-van Alphen effect in $LaSn_3$, J. Phys. Soc. Jpn. 60 (1991) 1294–1299.

[25] I. Umehara, Y. Kurosawa, N. Nagai, M. Kikuchi, K. Satoh, Y. Ōnuki, High field magnetoresistance and de Haas-van Alphen effect in $CeSn_3$, J. Phys. Soc. Jpn. 59 (1990) 2848–2855.

[26] Y. Ōnuki, R. Settai, De Haas-van Alphen effect and Fermi surface properties in rare earth and actinide compounds, Low. Temp. Phys. 38 (2012) 119–190.

[27] J.P. Sanchez, J.M. Friedt, G.K. Shenoyt, A. Percheron, J.C. Achard, Electronic and magnetic properties of rare-earth-Sn_3 compounds from ^{119}Sn Mössbauer spectroscopy, J. Phys. C. Solid State Phys. 9 (1976) 2207–2215.

[28] P. Blaha, K. Schwarz, G.K.H. Madsen, D. Kuasnicka, J. Luitz, WIEN2K, an Augmented Plane Wave + Local Orbitals Program for Calculating Crystal Properties, K. Schwarz, Technical Universitat, Wien, Austria, 2001.

[29] O.K. Andersen, Linear methods in band theory, Phys. Rev. B 12 (1975) 3060–3083.

[30] J.P. Perdew, A. Zuanger, Self-interaction correction to density functional approximations for many-electron systems, Phys. Rev. B 23 (1981) 5048–5079.

[31] S.J. Asadabadi, F. Kheradmand, Ab-initio prediction of magnetically dead layers in freestanding γ-Ce(111), J. Appl. Phys. 108 (2010) 073531.

[32] V.I. Anisimov, I.V. Solovyev, M.A. Korotin, M.T. Czyzyk, G.A. Sawatzky, Density-functional theory and NiO photoemission spectra, Phys. Rev. B 48 (1993) 16929–16934.

[33] D.D. Koelling, B.N. Harmon, A technique for relativistic spin polarized calculations, J. Phys. C. Solid State Phys. 10 (1977) 3107–3114.

[34] P. Novak, Calculation of Spin-orbit Coupling, (1997) http://www.wien2k.a/reg_user/textbooks/novak_lecture_on_spinorbit.ps.

[35] M. Iglesias, K. Schwarz, P. Blaha, D. Baldomir, Electronic structure and electric field gradient calculations of Al_2SiO_5 polymorphs, Phys. Chem. Miner. 28 (2001) 67–75.

[36] P. Blaha, K. Schwarz, P.H. Dederichs, First-principles calculation of the electric-field gradient in hcp metals, Phys. Rev. B 37 (1988) 2792–2796.

[37] N.D. Mathur, F.M. Grosche, S.R. Julian, I.R. Walker, D.M. Freye, R.K.W. Haselwimmer, G.G. Lonzarich, Magnetically mediated superconductivity in heavy fermion compounds, Nature 394 (1988) 39–43.

[38] Z. Kletowski, Examinations of phase transitions for $Nd(Sn, In)_3$ and $Sm(Sn, In)_3$ compounds by the electrical resistivity studies, Solid State Commun. 62 (1987) 745–747.

[39] K. Kawashima, M. Maruyama, M. Fukuma, J. Akimitsu, Superconducting state in YSn_3 with a $AuCu_3$-type structure, Phys. Rev. B 82 (2010) 094517.

[40] K. Betsuyaku, H. Harima, Electronic structure and electric field gradient of RIn_3 and $RTIn_5$ (R = La and Ce, T = Co, Rh and Ir), J. Magn. Magn. Mater. 272–276 (2004) 187–188.

[41] Y. Kohori, Y. Inoue, T. Kohara, G. Tomkaand, P.C. Riedi, ^{115}In NQR study in $CeIn_3$, Phys. B 281-282 (1999) 103–104.